RSC Advances

PAPER

View Article Online
View Journal | View Issue

Cite this: *RSC Adv.*, 2022, **12**, 19561

Controlled synthesis of open-mouthed epitope-imprinted polymer nanocapsules with a PEGylated nanocore and their application for fluorescence detection of target protein†

Xingjia Feng, Siyu Jin, Dongru Li and Guoqi Fu *

Epitope imprinting is an effective way to create artificial receptors for protein recognition. Surface imprinting with immobilized templates and sacrificial supports can generate high-quality imprinted cavities of homogeneous orientation and good accessibility, but it is still challenging to fabricate nanoscale imprinted materials by this approach. Herein, we propose a method for the controlled synthesis of open-mouthed epitope-imprinted polymer nanocapsules (OM-MIP NCs) by limiting the imprinting polymerization on the template-bearing side of the Janus nanoparticles (JNPs). Concurrent bromoacetyl (Ac–Br) and 2-bromoisobutyryl (iB–Br) functionalization of the major portion of SiO_2 nanoparticles is achieved *via* the molten-wax-in-water Pickering emulsion approach. The cysteinyl-derived epitope templates are immobilized through the Ac–Br groups, and then surface imprinting is fulfilled *via* ATRP initiated by the iB–Br groups. The SiO_2 supports are partially etched and then PEGlated, affording OM-MIP NCs with a PEGylated nanocore. The inside nanocore can facilitate collection of the NCs by centrifugation, and its PEGylation can inhibit non-specific binding. The surface imprinting can be optimized through the ATRP time, and the etching can be tailored *via* the concentration of NH_4HF_2 employed. For proof-of-concept, with a C-terminus nonapeptide of bovine serum albumin (BSA) chosen as a model epitope and polymerizable carbon dots added to the pre-polymerization solution, fluorescent OM-MIP NCs were fabricated for BSA sensing. The as-synthesized NCs exhibited satisfactory detection performance, with an imprinting factor of 6.1, a limit of detection of 38.1 nM, a linear range of 0.25–6 μM, and recoveries of 98.0 to 104.0% in bovine serum samples.

Received 9th April 2022
Accepted 27th June 2022

DOI: 10.1039/d2ra02298b

rsc.li/rsc-advances

Introduction

Molecular imprinting is a methodology for tailor-making receptors with antibody-like properties. Molecularly imprinted polymers (MIPs) are usually synthesized by copolymerization of functional and crosslinking monomers around template molecules. After template removal, specific cavities complementary to the template in size, shape and functionality are generated in the resultant polymer matrix. Compared with natural recognition materials like antibodies, MIPs show advantages such as thermal and chemical stability, low cost and ease of mass preparation. Therefore, MIPs have been widely used in various fields, such as affinity separation, sensors, bioanalysis, clinical therapy, and pharmacy.[1] The imprinting of proteins and other biomacromolecules is still challenged by their large size, complex structure and variable conformation.[2–5] Therefore, a variety of approaches, such as surface imprinting,[6–10] nanoscale imprinting,[11–13] solid synthesis[14,15] and epitope imprinting,[16–20] have been exploited to solve these problems.

With regard to epitope imprinting, an exposed amino acid sequence, glycan or monosaccharide of a target protein, rather than the whole biomacromolecule, is employed as the template for fabrication of MIPs.[17] Such epitope templates are not only more easily obtained by synthesis, but also much less susceptible to the harsh imprinting conditions, in comparison to protein molecules. Till now, epitope-imprinted materials have been utilized to recognize peptides, proteins and cells, and hence show potential applications in various areas, such as disease biomarker detection, recombinant protein purification, biosensors, cancer diagnosis and therapy.[16–25]

For synthesis of epitope-imprinted polymers, surface imprinting with immobilized templates and sacrificial the supports is an important way. It usually involves polymerization around the epitope templates orientedly immobilized on the surface of glass slides and other 2-D materials[26,27] or within the inner surface of macroporous silica spheres,[28–32] and hence the templates are fully encapsulated by the resultant polymers.

Key Laboratory of Functional Polymer Materials of Ministry of Education, Institute of Polymer Chemistry, College of Chemistry, Nankai University, Tianjin 300071, China. E-mail: gqfu@nankai.edu.cn; Tel: +86 22 23501443

† Electronic supplementary information (ESI) available. See https://doi.org/10.1039/d2ra02298b

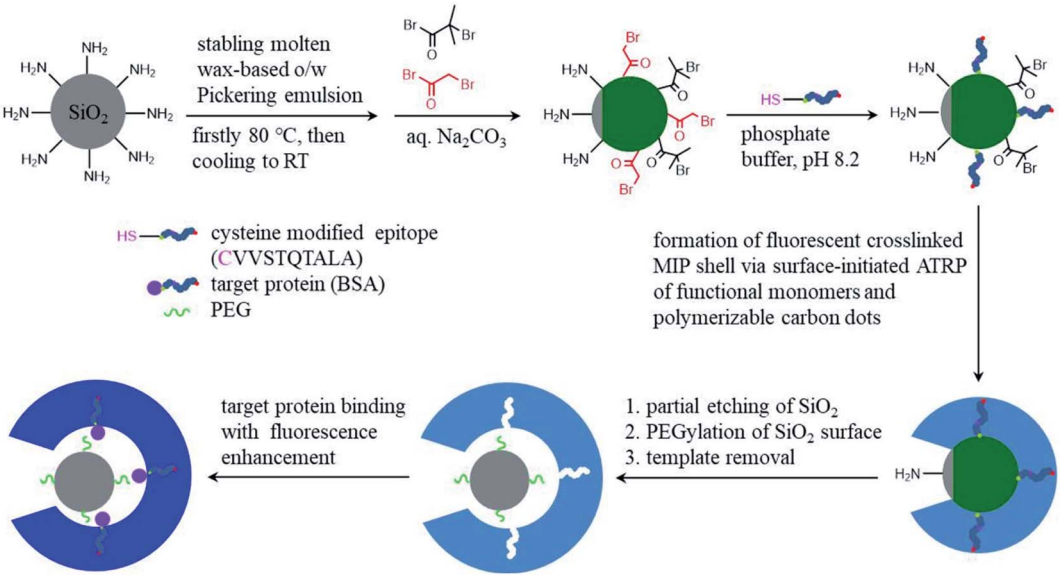

Scheme 1 Schematic illustration of the procedure for synthesis of open-mouthed epitope-imprinted polymer nanocapsules containing a PEGylated nanocore for FL detection of the target protein.

Afterwards, these supports are removed by etching or peeling, affording epitope-imprinted polymer films or spheres. The resultant high-quality imprinted cavities are featured with homogenous orientation and good accessibility. Besides epitope imprinting, such approach has also been successfully applied to imprinting of proteins[33–35] and small molecules.[36,37] However, it is still a challenge for the synthesis of nano-sized imprinted materials with high surface-to-volume ratio by this approach, which are highly desired in the applications such as biosensors, separation and drug delivery.[16–25] As such, we recently put forward a method for synthesis of open-mouthed epitope-imprinted polymer nanocapsules (OM-MIP NCs),[38] with asymmetrically functionalized SiO_2 Janus nanoparticles (JNPs) as the supports for the formation of incomplete imprinted polymer shells and then fully etched using NH_4HF_2 solution. The major surface of the JNPs is immobilized with both epitope templates and vinyl groups for subsequent surface imprinting *via* free radical polymerization (FRP), and the remaining surface grafted with polyethleneglycol (PEG) chains for prevention from local polymerization. The open-mouth of the OM-MIP NCs allows the target protein to freely get access to the oriented imprinted cavities on the inner surface. But this method is still suffered by some drawbacks. Firstly, the construction of the SiO_2 JNPs with multi-step of modification is rather tedious, attributed to the FRP employed. Secondly, the oriented immobilization of the epitope is achieved using glutaraldehyde as crosslinking agent, which only is adequate for the templates with only an amine at the terminus. Finally, the collection of the NCs cannot be conducted by a simple centrifugation due to their low density.

Aiming at the above problems, we demonstrate a surface-initiated AGET ATRP (SI-ATRP) based method for controlled synthesis of OM-MIP NCs containing a PEGylated SiO_2 nanocore of high density, which allows the OM-MIP NCs to be collected by centrifugation. As illustrated in Scheme 1, the SiO_2 JNPs used for surface imprinting were obtained simply by functionalization of the major portion of the amino-modified SiO_2 nanoparticles (NPs) concurrently with bromoacetyl (Ac–Br) and 2-bromoisobutyryl (iB–Br) groups. The Br–Ac groups were used to couple cysteinyl-derived epitope templates, a versatile approach for oriented epitope immobilization *via* the highly reactive thiol-bromoacetyl coupling chemistry. The Br-iB groups were employed to form surface imprinted polymer shells *via* SI-ATRP. After the imprinting polymerization, partial etching and subsequent PEGylation of the SiO_2 nanocores afforded the nanocore-containing OM-MIP NCs. Additionally, polymerizable carbon dots (CDs) were added to the pre-polymerization solution, so that the OM-MIP NCs were endowed with fluorescence (FL) response and their imprinting performance could be evaluated by FL detection.

Experimental

Materials

Tetraethylorthosilicate (TEOS), aminopropyltriethoxysilane (APTES), 5,5 -dithio -bis-(2-nitrobenzoic acid) (DTNB), tris(2-(dimethylamino)ethyl)amine (Me_6TREN) and 2-bromoisobutyryl bromide were purchased from Aladdin, China. Bromoacetyl bromide was purchased from J&K, China. *N*-isopropylacrylamide (NIPAm, recrystallized from hexane) was purchased from Acros Organics, Belgium. *N*-*tert*-butylacrylamide (TBAm) was purchased from Alfa Aesar, China. (3-Isocyanatopropyl)triethoxysilane (IPTES) were purchased from Heowns Biochem, China. Glycidyl methacrylate (GMA), copper bromide, ammonium hydrogen fluoride, ascorbic acid and ethylenediamine were obtained from Tianjin Chemical Reagents Co., China. Acrylamide (AAm, electrophoresis grade), *N*,*N*-methylenebisacrylamide (MBA, electrophoresis grade),

dodecyl sodium sulfate (SDS), paraffin wax (melting point: 50–52 °C), and cytochrome c (Cyt c) were purchased from Sangon, Shanghai. Bovine serum albumin (BSA), lysozyme (Lyz), human serum albumin (HSA), ovalbumin (OVA), trypsin were obtained from Sigma, China. Decapeptide (CVVSTQTALA) was provided by GL Biochem, China. Methoxy polyethylene glycol with an average molecular weight of 2000 (mPEG 2000) was purchased from Huateng Pharma, China. (*N*-triethoxysilylpropyl)-*O*-monomethoxy PEG urethane (silanated PEG) was synthesized with the mPEG 2000 according to the reference method.[39] 4-Acrylamidophenyl (amino)methaniminium chloride (AB) was synthesized according to the ref. 40 All the other chemicals were used as received unless otherwise stated. All aqueous solutions were prepared with ultrapure water (>18.6 MΩcm) produced by a UPR-II purification system (Chengdu YouPu Biotech Co., China). A phosphate buffer (pH 7.0, 10 mM) was denoted as PB.

Synthesis of vinyl functionalized CDs

The procedure for the synthesis of polymerizable CDs are shown in Scheme S1, ESI.† Firstly, CDs were synthesized according to the reference method.[41] Briefly, citric acid (5.26 g) and ethylenediamine (1.68 mL) dissolved in 50 mL of ultrapure water were transferred an teflon-lined autoclave (100 mL) and then the reaction was kept at 150 °C for 5 h. After cooling down to room temperature, brown-black and transparent CDs solution was obtained. Vinyl functionalization of the CDs was carried out according to a previously reported method[42] with some modification. The above CDs solution was mixed with 10 mL of GMA by magnetic stirring and the reaction was continued at 30 °C for 24 h. Then, the oil phase of the dispersion was removed, and the remaining water phase was further washed by n-hexane to remove the unreacted GMA molecules. Finally, vinyl functionalized CDs (denoted as GMA-CDs) were obtained by freeze-drying of the water solution.

Synthesis of epitope and ATRP initiator asymmetrically functionalized SiO_2 Janus nanoparticles

Firstly, SiO_2 NPs were synthesized by the Stöber method.[43] For amino-functionalization, the SiO_2 NPs (1.0 g) after dried were dispersed in anhydrous toluene (40 mL) containing APTES (0.8 mL), and then stirred at 30 °C for 8 h, followed by centrifugation and washing with ethanol and water. The resultant product was named as SiO_2–NH_2.

For bromoacetyl and 2-bromoisobutyryl functionalization of the major surface of the SiO_2–NH_2 NPs, SiO_2–NH_2 NPs coated wax spheres were firstly prepared by the molten-wax-in-water Pickering emulsion according the previously reported approach[44] with some modification. The SiO_2–NH_2 NPs (400 mg) were dispersed in water (40 mL). After adding wax (4 g), the dispersion was heated to 80 °C for melting the wax and mechanically stirred at 1500 rpm for 1 h, and then cooled to room temperature, resulting in the SiO_2–NH_2/wax colloidosomes. For bromo-modification of the exposed side of the SiO_2–NH_2 NPs, bromoacetyl bromide (36 μL, 400 μmol), and 2-bromoisobutyryl bromide (50 μL, 400 μmol) was added to the suspension at 4 °C under mechanical stirring (800 rpm), together with Na_2CO_3 (0.25 g) to maintain the pH at about 10. The reaction was continued RT for 12 h. The colloidosomes were collected by filtration, washed with methanol and water, and then dried. The resultant SiO_2–NH_2//Ac–Br/iB–Br Janus NPs (JNPs) were released from the colloidosomes by dissolving the wax with chloroform. For comparison, bromoacetyl and 2-bromoisobutyryl modified SiO_2 NPs (denoted as SiO_2-Ac-Br/iB–Br) was prepared by direct modification of the SiO_2–NH_2 NPs under the same conditions.

For epitope immobilization, the SiO_2–NH_2//Ac–Br/iB–Br JNPs were incubated in 14.4 mL of phosphate buffer (10 mM, pH 8.2, 5 mM EDTA, 150 mM NaCl) containing CVVSTATALA (8 mg, predissolved with 1.6 mL of DMF) at 30 °C for 6 h under argon, then washed with water, and finally freeze-dried. The resultant JNPs were denoted as SiO_2–NH_2//epitope/iB–Br. The epitope was also coupled to the SiO_2-Ac-Br/iB–Br NPs by the same way, and the resultant NPs were denoted as SiO_2- epitope/iB–Br.

Synthesis of fluorescent open-mouthed epitope-imprinted polymer nanocapsules containing a PEGylated core

Firstly, imprinted polymer shells were formed over the SiO_2–NH_2//epitope/iB–Br JNPs *via* SI-ATRP. The JNPs (50 mg) were incubated in 0.8 mL of the PB containing AB (1.54 mg, 0.002 mmol) at RT for 30 min. Afterwards, the JNPs were collected, and then incubated in 5 mL of the PB solution of NIPAm (167.45 mg, 1.48 mmol), MBA (65.19 mg, 0.423 mmol), AAm (12 mg, 0.169 mmol), TBAm (5.38 mg, 0.042 mmol) and GMA-CDs (4 mg) with a total monomer concentration of 5% (w/v) for 1 h at RT, followed by mixing with 0.2 mL of aqueous solution of $CuBr_2$ (2.24 mg, 0.01 mmol) and ME_6TREN (2.35 mg, 0.01 mmol). The reaction mixture was degassed under vacuum for 30 min and purged with argon. After 0.05 mL of aqueous solution of AsAc (0.88 mg, 0.005 mmol) was injected into the mixture, the ATRP was continued under magnetic stirring at 30 °C for 12 h. The as-prepared core–shell MIP JNPs were washed with 200 mM EDTA solution to remove residual Cu^{2+}, incubated in NH_4HF_2 solution (80 mM) containing 0.04% (w/v) of SDS at 30 °C for 24 h to partially etch the inside SiO_2 nanocores, followed by washing with 1 M NaCl solution and water to remove SDS. The as-obtained open-mouth NCs were stirred in 2 mL of HAc-NaAc buffer (20 mM, pH 4.0) containing the silanated PEG (10 mg) at 30 °C for 24 h for PEGylation of the inside SiO_2 nanocore. Finally, the NCs were washed with CH_3OH: acetic acid (9 : 1) for removal of the epitope template, with CH_3OH:16% ammonia water (3 : 7) for dissociating the carboxyl/amidine complex, and then freeze-dried before cleaning with water. The as-synthesized open-mouthed epitope-imprinted polymer nanocapsules containing a PEGylated nanocore were denoted as OM-MIP NCs. The non-imprinted polymer controls (OM-NIP NCs) were synthesized in the same way but using the SiO_2–NH_2//Ac–Br/iB–Br JNPs for SI-ATRP.

For comparison, the epitope-imprinted and non-imprinted polymer NCs without open mouths were also synthesized *via* the same procedure but using the SiO_2-epitope/iB–Br and SiO_2–Ac–Br/iB–Br NPs NPs as the supports for the ATRP, respectively.

The resultant products were denoted as closed MIP NCs and closed NIP NCs, respectively.

Characterization

FL spectra were recorded using a fluorospectrophotometer (F-2710, Hitachi, Japan), with the slit widths of excitation and emission set at 5 and 10 nm, respectively, and the photomultiplier tube voltage set at 700 V. All the samples (100 μg mL^{-1}) for FL measurements were dispersed by ultrasonication for several seconds with an ultrasonic cleaner (SB-3200 DTD, Ningbo SCIENTZ Biotech Co., China) in the PB unless stated otherwise. UV–Vis absorption was measured on a spectrophotometer (TU-1900, Purkinje General Instrument Co., China) equipped with a temperature controller. The morphologies and structures were observed by a TEM (Talos F200X G2, FEI, Netherlands) and a SEM (Apreo S LoVac, Thermoscientific, USA). The samples for TEM observation were dispersed in ethanol, cast onto carbon-coated 200-mesh copper grids, and then dried under vacuum. Zeta potentials and hydrodynamic diameters were measured by DLS (Zeta Sizer Nano-ZS90, Malvern, UK). Thermogravimetric analysis (TGA) was performed by a thermogravimetric analyzer (TG 209, NETZSCH, Germany) under nitrogen atmosphere with a heating rate of 10 °C min^{-1} up to 800 °C. FT-IR spectra were determined over KBr pellets on a FT-IR spectrometer (Nicolet iS50, ThermoFisher Scientific, USA).

Analysis of real samples

Fetal bovine serum was employed to examine the practicability and accuracy of the imprinted NCs for target protein detection. Briefly, the bovine serum was diluted 1000-fold with the PB. The imprinted NCs (100 μg) were added into the diluted bovine serum solution (1 mL) spiked with the target protein at four concentration levels. The FL spectra of the dispersion were recorded and all the tests were performed in triplicates.

Results and discussion

Synthesis and characterization of fluorescent OM-MIP NCs containing a PEGylated core

The molten-wax-based o/w Pickering emulsion technique is a very effective method to fabricate Janus colloidal particles with controllable surface properties and, moreover, is readily scaled up.[45,46] Asymmetrical functionalization of SiO_2–NH_2 NPs was performed by the approach reported by Berger *et al.*[44] with some modification, and the resultant JNPs were used as the sacrificial nanosupports for construction of OM-MIP NCs. As shown in Scheme 1, the SiO_2–NH_2 NPs were used to stabilize molten-wax-in-water emulsion, and their minor surface was embedded in wax spheres after cooling down the emulsion. The exposed part of the SiO_2–NH_2 NPs were concurrently modified with both 2-bromoisobutyryl bromide and 2-bromoacetyl bromide, and then SiO_2–NH_2//Ac–Br/iB–Br JNPs were afforded after dissolution of the wax. Herein, the C-terminus nonapeptide (VVSTQTALA) of BSA was chosen as a model epitope template to prepare OM-MIP NCs for BSA recognition. The cysteinyl derivative (CVVSTQTALA) of the epitope was coupled to the JNPs principally through the Ac–Br groups by the effective thiol–bromoacetyl coupling reaction. The as-prepared JNPs were incubated in an AB monomer solution for the formation of strong interactions between the amidine moiety and the C-terminus carboxylate group of the immobilized peptide.[27] Then, surface imprinting over the epitope-bearing side of the JNPs was achieved through the iB–Br groups by SI-ATRP of NIPAm, TBAm, AAm, GMA-CDs, and MBA as a crosslinker. In the pre-polymerization solution, NIPAm was used as main monomer which can both form hydrogen bonds with the epitope and make the resulting imprinted coatings thermos-responsive. As the assistant functional monomers, TBAm and AAm can interact with the epitope *via* hydrophobic association and hydrogen bonding, respectively. GMA-CDs were introduced for integration of their FL response properties into the imprinted coatings and hence the imprinting performance could be evaluated by FL measurements. On the contrary, the polymerization could not be initiated over the minor side of the JNPs with only –NH_2 groups. Therefore, the OM-MIP NCs containing a nanocore were obtained after limited etching and then PEGylation of the SiO_2 JNPs, because that the residual SiO_2 NPs, if over etched, could escape out of the NCs from the mouth, and the PEGylation could restrain non-specific binding to the surface of the etched SiO_2 NPs.

In our previous study on hollow OM-MIP NCs,[38] the oriented immobilization of the BSA epitope was accomplished through the only one amine group at the N-terminus with glutaraldehyde as a coupling agent. However, this approach does not

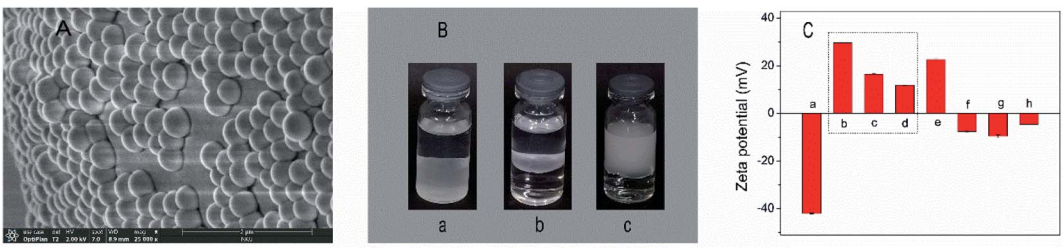

Fig. 1 (A) SEM image of the wax colloidosomes coated by SiO_2–NH_2 NPs. (B) Photographs showing the locations of SiO_2–NH_2 NPs (a), SiO_2–NH_2//Ac–Br/iB–Br JNPs (b) and SiO_2–Ac–Br/iB–Br NPs (c) added to a dual-phase system of dichloromethane and water. (C) The zeta potentials of pristine SiO_2 NPs (a), SiO_2–NH_2 NPs (b), SiO_2–NH_2//Ac–Br/iB–Br JNPs (c), SiO_2–Ac–Br/iB–Br NPs (d), SiO_2–NH_2//Ac-epitope/iB–Br JNPs (e), MIP JNPs (f), OM-MIP NCs before PEGylation of the partially etched SiO_2 core (g), and OM-MIP NCs (h).

work, if an epitope sequence bears multiple amine groups. Obviously, the present oriented epitope immobilization *via* the thiol-bromoacetyl coupling chemistry is rather versatile. Moreover, the utilization of SI-ATRP brings about much simpler surface functionalization and controllable imprinting polymerization, in comparison with the FRP based method. Also, with a partially etched and PEGylated SiO_2 nanocore inside, the OM-MIP NCs can be facilely handled by centrifugation, hence avoiding time-consuming and tedious dialysis of the hollow OM-MIP NCs for either template removal or washing.

The original SiO_2 NPs synthesized *via* the Stöber method[43] were rather uniform with an average size of about 318 nm (Fig. S1a, ESI†). The SiO_2 NPs were modified with APTES, resulting in SiO_2–NH_2 NPs. The minor portion of the SiO_2–NH_2 NPs were masked by the solidified wax spheres following the Pickering emulsion approach,[44] as shown in Fig. 1A. Based on the SiO_2–NH_2 NPs of about 800 nm in diameter, Berger *et al.*[44] confirmed the successful asymmetrical acylation of the exposed amine groups pointing to water phase with 2-bromoisobutyryl bromide by fluorescence microscopy and environmental scanning electron microscope. Regrettedly, the colloid particles of about 300 nm in this work are too small to be characterized by these ways. However, the asymmetrical surface functionalization was supported by the location of the SiO_2–NH_2//Ac–Br/iB–Br JNPs different from that of the uniformly modified particles, SiO_2–NH_2 and SiO_2–Ac–Br/iB–Br NPs, added in a dual-phase mixture of dichloromethane and water.[47] As shown in Fig. 1B, the SiO_2–NH_2 NPs were well dispersed in the bottom dichloromethane phase due to the relatively hydrophobic surface and the hydrophilic SiO_2–Br–Ac/Br–iB NPs in the top water phase; while the SiO_2–NH_2//Br–Ac/Br–iB JNPs were located at the water/dichloromethane phase interface due to the disparity in the hydrophilic/hydrophobic properties of the two sides. As shown in Fig. 1C, the zeta potential of the JNPs was measured to be between that of SiO_2–NH_2 and SiO_2–Ac–Br/iB–Br NPs, further supporting their Janus surface characteristics. The surface modification was also proved by the FT-IR spectra of these particles (see Fig. S2, ESI†).

The amount of the cysteinyl derived epitope (CVVSTQTALA) immobilized to the SiO_2–NH_2//Ac–Br/iB–Br JNPs was determined to be ~4.8 μmol g^{-1}, by analyzing the thiol contents of the peptide sequence solutions before and after the coupling reactionfollowing the Ellman's method.[48] The sequence may be anchored primarily through the Br–Ac groups, in comparison with the less active Br-iB groups due to high steric hindrance. Hence, the Br-iB groups can be left behind enough to initiate the following ATRP for surface imprinting. This assumption was proved by comparing the sequence amounts coupled to the JNPs with that to the NPs obtained by functionalization of the SiO_2–NH_2 NPs with 2-bromoisobutyryl bromide, 2-bromoacetyl bromide, and 2-bromoisobutyryl bromide/2-bromoacetyl bromide (molar ratio of 1 : 1), respectively, under the same reaction conditions (see Fig. 2A). The coupled amounts were determined to be 2.0, 7.9 and 6.2 μmol g^{-1}, respectively. In addition, the amount coupled to the Ac–Br and iB–Br modified SiO_2–NH_2 NPs, 6.2 μmol g^{-1}, is significantly higher than the amount (4.8 μmol g^{-1}) coupled to the SiO_2–NH_2//Ac–Br/iB–Br JNPs, further proving their Janus surface, since the epitope cannot be attached to the amine-bearing side.

Surface imprinting polymerization over the SiO_2–NH_2//epitope/iB–Br JNPs was initiated primarily from the iB–Br groups, followed by partial etching the SiO_2 nanocores in dilute NH_4HF_2 solution. The TGA curves of different particles were measured, as shown in Fig. 2B. According to the residual weight percentage of the MIP JNPs and SiO_2–NH_2//epitope/iB–Br JNPs (w_2 and w_1, respectively), the mass of polymer shells relative to the cores was calculated to ~4.2% ($w_2/w_1 - 1$). The resultant OM-MIP NCs showed further decreased residual weight, hence proving partial etching of SiO_2 core. As seen from the TEM images (Fig. S1, ESI†), the MIP JNPs and OM-MIP NCs remained uniform spherical morphology like that of original SiO_2 NPs, but the imprinted polymer shells could not be discriminated clearly, probably due to the shrinking of the thin polymer shells while dried. Hence, it is not surprising that the open-mouth of the OM-MIP NCs could be distinguished from neither the TEM images nor SEM photographs (data not shown). According to the TEM images, the average diameters of the MIP JNPs, OM-MIP NCs and original SiO_2 NPs were counted to be 327, 304 and 318 nm, respectively. Therefore, the thickness of the imprinted polymer shells was estimated to be about 4.5 nm ((327–318)/2) from the sizes of the MIP JNPs and SiO_2 NPs. The SiO_2 core inside the MIP JNPs was reduced by 11.5 nm ((327–304)/2) in radius, as estimated from the sizes of the MIP JNPs and OM-MIP NCs. Obviously, this gap size within the OM-MIP

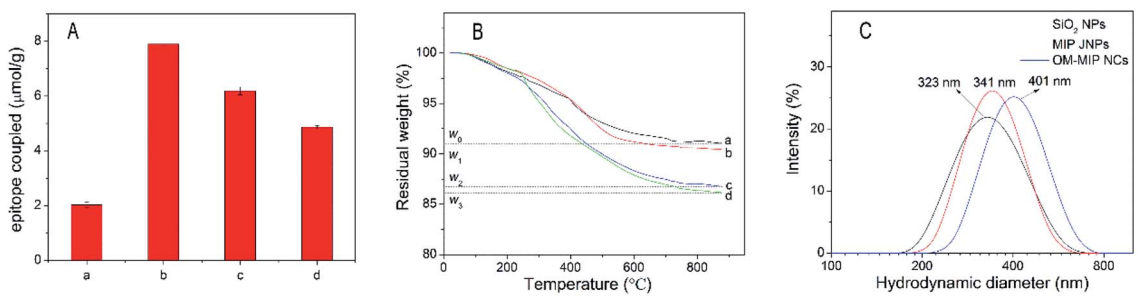

Fig. 2 (A) The amounts of the epitope coupled to SiO_2–iB–Br NPs (a), SiO_2–Ac–Br NPs (b), SiO_2–Ac–Br/iB–Br NPs (c) and SiO_2–NH_2//Ac–Br/iB–Br JNPs (d). (B) TGA curves of SiO_2 NPs (a), SiO_2–NH_2//epitope/iB–Br JNPs (b), MIP JNPs (c), and OM-MIP NCs with template removed but without PEGylated (d). (C) The hydrodynamic diameters of SiO_2 NPs (black line), MIP JNPs (red line) and OM-MIP NCs (blue line) in water.

NCs would not be large enough for the BSA molecules of about 8 nm in size[49] to freely get access to the inside imprinted cavities from the open mouth. Furthermore, the average hydrodynamic diameters (D_h) of the MIP JNPs, OM-MIP NCs and original SiO_2 NPs were measured in water *via* DLS to be 341, 401 and 323 nm, respectively (see Fig. 2C). Therefore, the imprinted shell thickness of the MIP JNPs was swollen to about 9 nm. The D_h of the OM-MIP NCs is 60 nm larger than that of the MIP JNPs, indicative of that the imprinted shells in the swollen state would become significantly enlarged after destroying the covalent linkage to SiO_2 core beneath. Hence, the gap size inside the OM-MIP NCs would increase up to 30 nm, pretty favorable for the target protein molecules to diffuse to the imprinted cavities within the inner surface from the open mouth. On the other hand, the OM-MIP NCs showed temperature-responsiveness, with a volume phase transition temperature (VPTT) determined to be about 37 °C (see Fig. S3, ESI†).

Optimal synthesis of the imprinted polymer nanocapsules

In the imprinting polymerization solution, polymerisable CDs (GMA-CDs) were added for integration of the specific recognition of the epitope-imprinted NCs and the FL sensing property of CDs. The GMA-CDs showed a size less than 2 nm, and illustrated relatively wide FL excitation and emission spectra (Fig. S4, ESI†). The CDs embedded OM-MIP NCs showed the strongest FL emission at $\lambda_{ex} = 350$ nm and could remain stable FL emission up to 120 min (Fig. S5, ESI†). As shown from Fig. 3A, the OM-MIP NCs showed an emission peak at λ_{em} of 447 nm. It is worthwhile to note that, the OM-MIP NCs showed FL enhancement, rather than FL quenching, in the presence of BSA. Therefore, such FL sensors based on molecular imprinting are called a "turn-on" type, which is favorable for sensitive and selective detection with less interference by the background FL in comparison with the "turn-off" type.[50] Also, the FL response mechanism could be attributed to the photo-induced electron transfer (PET) between the CDs and the protein, since the FL emission spectra of the OM-MIP NCs did not overlap with the absorption spectrum of BSA.[50]

The FL enhancement is expressed as $F/F_0 - 1$, where F_0 and F are the FL intensities in the absence and presence of an analyst, respectively. The ratio of $F/F_0 - 1$ for a MIP relative to that for the corresponding NIP, denoted as $(F/F_0 - 1)_{MIP/NIP}$, can be employed to evaluate the FL response of the MIP due to the specific binding to the imprinting sites. According to $(F/F_0 - 1)_{MIP/NIP}$, the conditions employed for synthesis of the FL OM-MIP NCs, such as the mass ratio of GMA-CDs relative to the nanocores (SiO_2–NH_2//epitope/iB–Br or SiO_2–NH_2//Ac–Br/iB–Br JNPs) and crosslinking degree (molar ratio of MBA relative to the total monomers), were optimized (Fig. S6, ESI†). Also, the temperature and pH value used for FL detection of protein were optimized to be 25 °C and pH 7, respectively (Fig. S7, ESI†).

The thickness of the imprinted NCs with GMA-CDs embedded may affect their FL response properties. The SI-ATRP from the JNPs bearing iB–Br groups could provide a more facile avenue for control of the thickness by polymerization time, compared with the FRP employed previously.[38] As shown in Fig. 3B, the OM-MIP NCs showed the highest level of $(F/F_0 - 1)_{MIP/NIP}$ at 12 h. The FL intensities of the corresponding MIP JNPs before SiO_2 etching increased with prolonging the polymerization time (see Fig. 3C), hence indicating gradual increase in the thickness of the imprinted polymer shells.

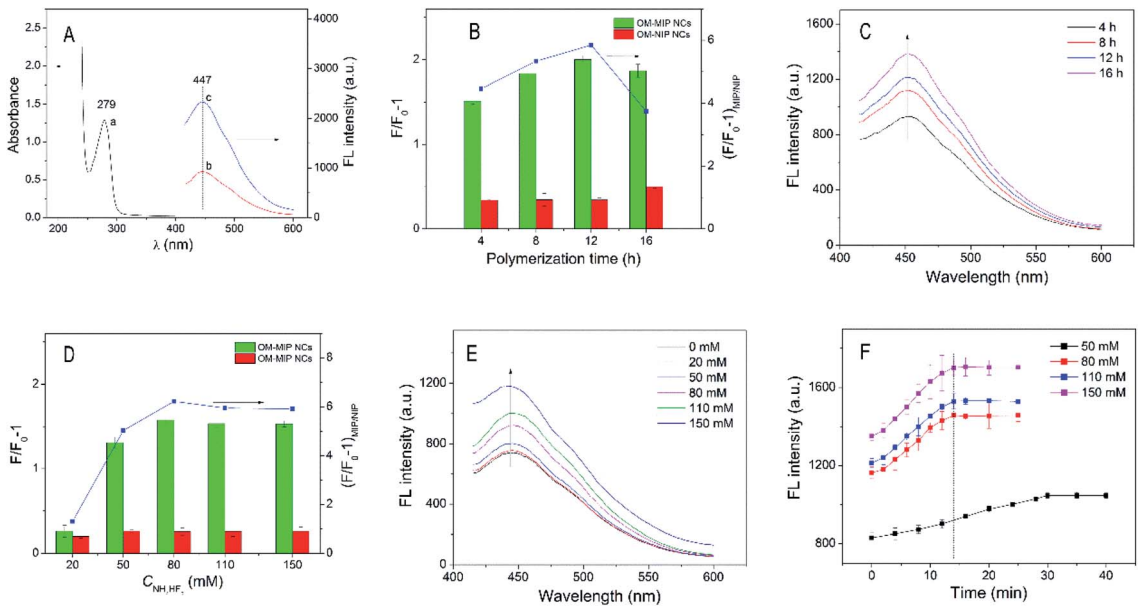

Fig. 3 (A) The absorption spectrum of BSA (a), and FL emission spectra of the OM-MIP NCs in the absence of BSA (b) and in the presence of BSA (3 μM) (c) at $\lambda_{ex} = 350$ nm. (B) The effect of polymerization time on the FL response of the resultant OM-MIP NCs and OM-NIP NCs. (C) The FL intensities of the MIP JNPs produced with different polymerization times. (D) The effect of $C_{NH_4HF_2}$ employed for the etching on the FL response of the resultant OM-MIP NCs and OM-NIP NCs. (E) The FL intensities of the OM-MIP NCs (non-PEGylated) produced with different $C_{NH_4HF_2}$ for the etching. (F) The FL response kinetics of the OM-MIP NCs in the presence of BSA (3 μM) produced with different $C_{NH_4HF_2}$ for the etching.

The partial etching of the SiO_2 core inside the MIP JNPs was controlled by gradual raising the NH_4HF_2 concentration ($C_{NH_4HF_2}$) with the same other reaction conditions. As seen from Fig. 3D, the $(F/F_0 - 1)_{MIP/NIP}$ of the OM-MIP NCs initially increased gradually and then leveled off when the $C_{NH_4HF_2}$ reached 80 mM. As shown in Fig. 3E, the FL intensities of the OM-MIP NCs continued increasing with increase of the $C_{NH_4HF_2}$, thus proving that higher $C_{NH_4HF_2}$, the more of the SiO_2 core was dissolved. The FL response kinetics of the OM-MIP NCs obtained with increasing $C_{NH_4HF_2}$ was further examined. As shown in Fig. 3F, after the $C_{NH_4HF_2}$ reached 80 mM, all the OM-MIP NCs achieved the stable FL response within about 14 min. This FL response speed is comparable to that of the hollow OM-MIP NCs reported in our previous study.[38] This result indicated that, the residual SiO_2 core inside OM-MIP NCs after etching with 80 mM of NH_4HF_2 no longer hindered the protein molecules to approach the imprinted cavities located at the inner surface from the open mouth, and hence this concertation was chosen in the following study. On the other hand, closed MIP NCs as well as NIP NCs were also synthesized *via* the same method for the OM-MIP NCs, except for polymerization over the uniformly functionalized NPs. It spent up to 80 min for these closed NCs to reach the highest FL response (Fig. S8, ESI†), since the protein molecules had to diffuse across the cross-linked polymer shells to access the imprinted cavities generated on the inner surface. This result, consistent with that found with the hollow OM-MIP NCs synthesized *via* FRP,[35] indicated the existence of the open mouth on the OM-MIP NCs.

PEGylation of the partially etched SiO_2 core

Inside the OM-MIP NCs, the partially etched SiO_2 nanocore with plenty of silanol groups would bring about non-specific binding, and hence affect the FL response properties. It is well known that surface PEGylation can effectively restrain non-specific binding.[51] Thus, we firstly tried a PEG-derived silane coupling agent for surface functionalization of the original SiO_2 NPs, together with these after etched with 80 mM of NH_4HF_2 for comparison. The surface of the etched SiO_2 NPs was more coarse than the untreated, as seen from the SEM images (Fig. S9, ESI†). These NPs were PEGlated with the PEG silane and then tested for BSA binding. Successful PEGylation was confirmed by the TGA (Fig. S10, ESI†). As shown in Fig. 4a, before PEGylation, the etched NPs exhibited about 3 times higher BSA binding than the un-etched NPs, primarily due to the larger surface area. However, the BSA binding to both NPs was decreased to less than 5 mg g^{-1}. Therefore, the OM-MIP NCs containing the etched SiO_2 core were PEGylated by incubation in the aqueous solution of the silanated PEG. The successful PEGylation was confirmed by FT-IR analysis (see Fig. S2, ESI†). It was proved that such PEGylation could significantly improve the FL response of the OM-MIP NCs, as can be seen from Fig. 4b, with the $(F/F_0 - 1)_{MIP/NIP}$ increased from 3.3 to 5.7.

Fluorescence sensing performance

The FL spectra of both the OM-MIP and OM-NIP NCs were recorded with the BSA concentrations ranging from 0 to 6 μM, for examining their ability for sensitive detection of the target protein. As shown in Fig. 5a and b, the OM-MIP NCs showed remarkably higher FL enhancement response to BSA than the corresponding OM-NIP NCs, attributed to the epitope-imprinted cavities generated on the inner surface of the OM-MIP NCs. The FL enhancement $(F/F_0 - 1)$, as defined above, should follow the Stern–Volmer equation

$$F/F_0 - 1 = K_{sv}\, C \quad (1)$$

where K_{SV} is the Stern–Volmer constant, and C is the of the target protein concentration.[52,53] The ratio of $K_{SV,MIP}/K_{SV,NIP}$ is defined as imprinting factor (IF_{SV}). In the concentration range covered, $F/F_0 - 1$ for both OM-MIP and OM-NIP NCs was well fitted to the Stern–Volmer equation, yielding correlation coefficients up to 0.999. The K_{sv} values were estimated to be 0.515 and 0.084 μM^{-1} for the OM-MIP and OM-NIP NCs, respectively, and hence the IF_{SV} for the OM-NIP NPs was calculated to be 6.13. The limit of detection (LOD) for the OM-MIP NCs were determined to be 38.1 nM, according to $3\sigma/s$,[52–57] where σ means the standard deviation of the blank measurements ($n = 11$) and s the slope of calibration curve ($s = K_{sv}$). For comparison, the FL

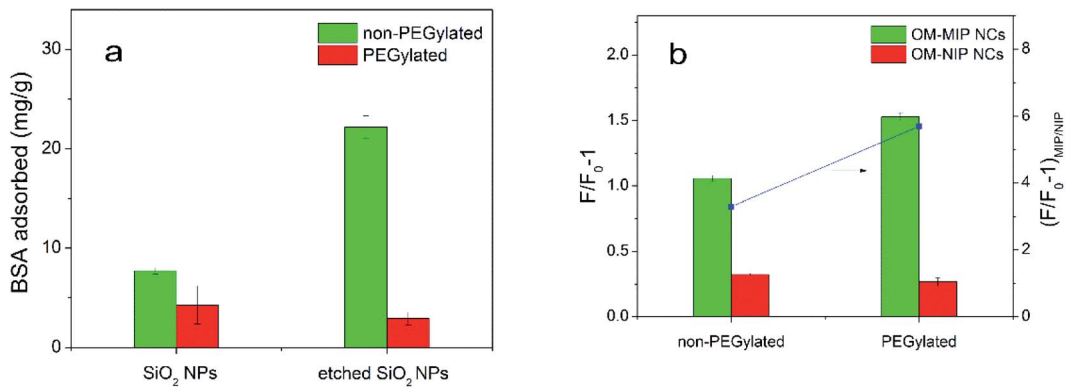

Fig. 4 (a) BSA binding amounts to the SiO_2 NPs treated differently, and (b) FL response of the OM-MIP NCs and OM-NIP NCs before and after PEGylation of the inside SiO_2 core.

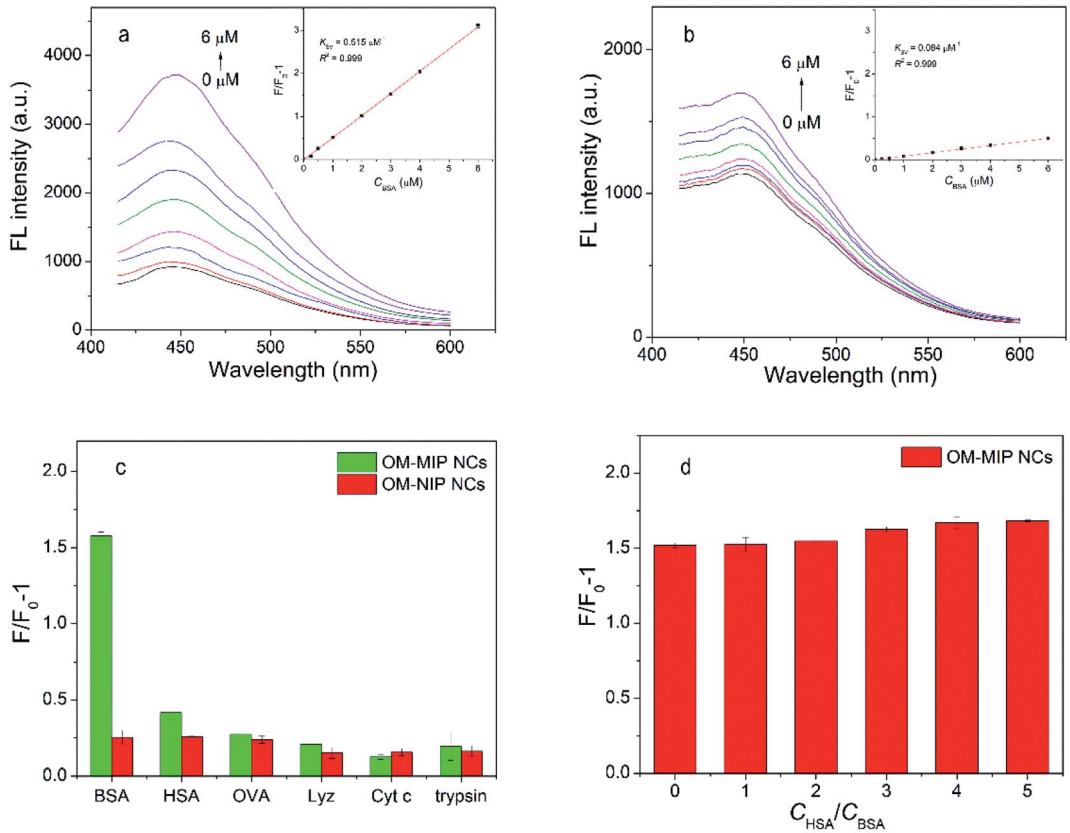

Fig. 5 FL emission spectra of (a) OM-MIP NCs and (b) OM-NIP NCs in the presence of BSA (0–6 μM), respectively. The insets show the corresponding Stern–Volmer plots. (c) FL response of OM-MIP and OM-NIP NCs in the presence of different proteins (3 μM). (d) FL response of the OM-MIP NCs to BSA (3 μM) mixed with HSA of multifold higher concentrations.

spectra of the OM-MIP and OM-NIP NCs without PEGylation were also measured (Fig. S11, ESI†). A lower IF_{SV} of 3.27 and a higher LOD of 81.7 nM were yielded, hence further proving that the PEGylation was necessary for enhancing the FL sensing performance of the OM-MIP NCs.

Considering both IF_{SV} and LOD, the OM-MIP NCs synthesized in this work showed much better performance than the other epitope or protein-imprinted FL sensors for BSA or HSA detection reported previously (Table S1, ESI†). This can be attributed to the high-quality epitope-imprinted cavities orientedly generated on the inner surface of the open-mouthed NCs. It is noted that their performance was comparable to that of our previous hollow OM-MIP NCs fabricated *via* FRP,[38] rather than greatly improved. This may be explained by assuming that, the present OM-MIP NCs were synthesized *via* SI-ATRP at a temperature of 30 °C, below the VPTT (37 °C), hence following a solution polymerization (SP) mechanism, while the hollow NCs were obtained *via* FRP-based precipitation polymerization (PP). We found that the protein-imprinted NPs synthesized *via* PP exhibited better recognition properties than those *via* SP, owing to the reversible physical cross-links created within the thermo-responsive polymer matrix.[58,59] This will be carefully examined in the future study. For all that, the present SI-ATRP-based approach significantly outperforms the previous FRP-based one, in terms of the generality for oriented coupling of epitope templates, simpleness in construction of the sacrificial JNPs and control of the polymerization, and facile collection of the NCs.

The FL response selectivity of the OM-MIP NCs for BSA was tested using other reference proteins having different M_w and isoelectric point (pI) with a same concentration (3 μM). The M_w and pI all the proteins used are BSA (M_w 67 k, pI 4.8), HSA (M_w 66 k, pI 4.8), OVA (M_w 44.5 k, pI 4.5), Lyz (M_w 14 k, pI 11.1), Cyt c (M_w 12.4 k, pI 10.2), trypsin (M_w 24 k, pI 10.5). It is worthy of noting that BSA and HSA are homologous proteins sharing approximately 80% amino acid identity.[60] Therefore, with HSA as a reference protein can severely test the FL recognition selectivity of the imprinted materials against the epitope of BSA. As shown in Fig. 5c, the OM-MIP NCs showed much higher $F/F_0 - 1$ toward BSA than toward HSA and other reference proteins, and also exhibited much higher $F/F_0 - 1$ level than that of the OM-NIP NCs toward all the investigated proteins. Moreover, the FL response of the OM-MIP NCs toward BSA (3 μM) was almost not influenced by mixing with HSA (up to five-fold higher concentration) (Fig. 5d).

The OM-MIP NCs were further used as FL sensors to detection of BSA in diluted bovine serum samples spiked with different BSA concentrations. The bovine serum was 1000-fold diluted so as to lower the BSA concentration within the linear range of the calibration curve obtained above. Satisfactory

recoveries and accuracies were achieved with a recovery range of 98.0–104.0% and RSDs of 1.2–4.6% for the spiked samples with four concentrations (Table S2, ESI†). Therefore, the OM-MIP NCs may be potentially applied for accurate and sensitive detection of low BSA concentrations in real bio-samples.

Reusability of the OM-MIP NCs

The OM-MIP NCs after binding of BSA for FL measurements were regenerated by sequential washing with 1% SDS/1% acetic acid solution to remove the bound protein, with 1 M NaCl solution to clear the SDS and finally with water. The as-regenerated OM-MIP NCs were reused for the FL analysis. The FL response of the MIP NPs to BSA remained almost intact after up to four use/regeneration cycles (Fig. S12, ESI†). This indicated that such imprinted mamomaterials have relatively good chemical stability against the template removal agent. Furthermore, the reuse of the MIPs means possible reduction of the practical use cost.

Conclusions

In summary, we have demonstrated a versatile method for controlled synthesis of oriented surface epitope-imprinted open-mouthed polymer NCs with a PEGylated nanocore for target protein recognition. This was based on surface imprinting polymerization over the SiO_2 JNPs, with the major surface coupled with both ATRP initiator and cysteinyl-derived epitope templates, followed by partial etching and PEGylating of the SiO_2 nanosupport. With a C-terminus nonapeptide of BSA as a model epitope and polymerizable carbon dots added to the imprinting polymerization system, the resultant OM-MIP NCs exhibited satisfactory performance for FL detection of BSA, with an imprinting factor of 6.1, a limit of detection of 38.1 nM, and spiked recoveries of 98.0 to 104.0% in bovine serum samples. Such OM-MIP NCs may potentially be applied to construction of other kinds of biosensors such as SPR and QCM. Also, this method may be further extended to imprint small molecules or biomacromolecules like proteins.

Compared with our recently reported method for synthesis of hollow OM-MIP NCs *via* FRP, the present method is featured with several advantages as follows. It is a versatile way for oriented immobilization of epitope templated *via* the highly efficient thiol-bromoacetyl reaction. The construction of the SiO_2 JNPs for surface imprinting becomes relatively simplified. Collection of the OM-MIP NCs can be readily performed by centrifugation, attributed to the inside PEGylated SiO_2 core. Additionally, the fabrication procedure consisting of the SI-ATRP and partial SiO_2 etching is controllable.

As for synthesis of epitope-imprinted polymers by surface imprinting with immobilized templates and sacrificial the supports, this work demonstrated an effective way for the construction of nano-sized imprinted materials, in contrast to the previous studies reporting much larger imprinted films or microspheres.[26–32] Moreover, the Pickering emulsion technique employed for the synthesis of the SiO_2 JNPs is considered to be readily scaled up.[45,46] However, the tedious multi-step procedure remains to be improved.

Author contributions

Xingjia Feng: investigation, methodology, validation and writing (original draft). Siyu Jin: investigation. Dongru Li: investigation. Guoqi Fu: conceptualization, methodology, writing (review & editing), supervision and funding acquisition.

Conflicts of interest

There are no conflicts to declare.

Acknowledgements

This work was supported by the National Natural Science Foundation of China (No. 21674051) and the National Key R&D Program of China (2020YFC1808603).

Notes and references

1 L. X. Chen, S. F. Xu and J. H. Li, *Chem. Soc. Rev.*, 2011, **40**, 2922–2942.
2 D. R. Kryscio and N. A. Peppas, *Acta Biomater.*, 2012, **8**, 461–473.
3 S. J Li, S. S. Cao, M. J. Whitcombe and S. A. Piletsky, *Prog. Polym. Sci.*, 2013, **39**, 145–163.
4 M. Dabrowski, P. Lach, M. Cieplak and W. Kutner, *Biosens. Bioelectron.*, 2018, **102**, 17–26.
5 Y. T. He and Z. A. Lin, *J. Mater. Chem. B*, DOI: **10.1039/D2TB00273F**.
6 T. Shiomi, M. Matsui, F. Mizukami and K. Sakaguchi, *Biomaterials*, 2005, **26**, 5564–5571.
7 A. Nematollahzadeh, W. Sun, C. S. A. Aureliano, D. Lutkemeyer, J. Stute, M. J. Abdekhodaie, A. Shojaei and B. Sellergren, *Angew. Chem., Int. Ed.*, 2011, **50**, 495–498.
8 X. T. Shen, T. C. Zhou and L. Ye, *Chem. Commun.*, 2012, **48**, 8198–8200.
9 Y. Q. Lv, T. W. Tan and F. Svec, *Biotechnol. Adv.*, 2013, **31**, 1172–1186.
10 M. F. Pan, L. P. Hong, X. Q. Xie, K. X. Liu, J. Y. Yang and S. Wang, *Macromol. Chem. Phys.*, 2021, **222**, 2000222.
11 Y. Hoshino, T. Kodama, Y. Okahata and K. J. Shea, *J. Am. Chem. Soc.*, 2008, **130**, 15242–15243.
12 A. Cutivet, C. Schembri, J. Kovensky and K. Haupt, *J. Am. Chem. Soc.*, 2009, **131**, 14699–14702.
13 T. Takeuchi, Y. Kitayama, R. Sasao, T. Yamada, K. Toh, Y. Matsumoto and K. Kataoka, *Angew. Chem., Int. Ed.*, 2017, **56**, 7088–7092.
14 S. Ambrosini, S. Beyazit, K. Haupt and B. T. S. Bui, *Chem. Commun.*, 2013, **49**, 6746–6748.
15 R. Mahajan, M. Rouhi, S. Shinde, T. Bedwell, A. Incel, L. Mavliutova, S. Piletsky, I. A. Nicholls and B. Sellergren, *Angew. Chem., Int. Ed.*, 2019, **58**, 727–730.
16 S. Dietl, H. Sobek and B. Mizaikoff, *Trends Anal. Chem.*, 2021, **143**, 116414.
17 K. G. Yang, S. W. Li, L. K. Liu, Y. W. Chen, W. Zhou, J. Q. Pei, Z. Liang, L. H. Zhang and Y. K. Zhang, *Adv. Mater.*, 2019, **31**, 1902048.

18 S. P. B. Teixeira, R. L. Reis, N. A. Peppas, M. E. Gomes and R. M. A. Domingues, *Sci. Adv.*, 2021, **7**, eabi9884.
19 M. Harijan, V. Shukla, A. Kumar Singh, R. Raghuwanshi, G. Nath and M. Singh, *Biosens. Bioelectron.: X*, 2022, **10**, 100090.
20 S. A. Piletsky, T. S. Bedwell, R. Paoletti, K. Karim, F. Canfarotta, R. Norman, D. J. L. Jones, N. W. Turner and E. V. Piletska, *J. Mater. Chem. B*, DOI: 10.1039/D2TB00278G.
21 K. Haupt, P. X. M. Rangel and B. T. S Bui, *Chem. Rev.*, 2020, **120**, 9554–9582.
22 S. X. Xu, L. S. Wang and Z. Liu, *Angew. Chem., Int. Ed.*, 2021, **60**, 3858–3869.
23 J. M. Pan, W. Chen, Y. Ma and G. Q. Pan, *Chem. Soc. Rev.*, 2018, **47**, 5574–5587.
24 X. D. Wang, G. Chen, P. Zhang and Q. Jia, *Anal. Methods*, 2021, **13**, 1660–1671.
25 T. Khumsap, A. Corpuz and L. T. Nguyen, *RSC Adv.*, 2021, **11**, 11403–11414.
26 H. Nishino, C. S. Huang and K. J. Shea, *Angew. Chem., Int. Ed.*, 2006, **45**, 2392–2396.
27 G. Q. Pan, S. Shinde, S. Y. Yeung, M. Jakstaite, Q. J. Li, A. G. Wingren and B. Sellergren, *Angew. Chem., Int. Ed.*, 2017, **129**, 16175–16179.
28 M. M. Titirici and B. Sellergren, *Anal. Bioanal. Chem.*, 2004, **378**, 1913–1921.
29 X. Yang, X. C. Dong, K. Zhang, F. F. Yang and Z. C. Guo, *J. Mater. Chem. B*, 2016, **4**, 920–928.
30 F. F. Yang, D. D. Deng, X. C. Dong and S. Lin, *J. Chromatogr., A*, 2017, **1494**, 18–26.
31 L. N. Gómez-Arribas, M. M. Darder, N. García, Y. Rodriguez, J. L. Urraca and M. C. Moreno-Bondi, *ACS Appl. Mater. Interfaces*, 2020, **12**, 49111–49121.
32 L. N. Gómez-Arribas, J. L. Urraca, E. Benito-Peña and M. C. Moreno-Bondi, *Anal. Chem.*, 2019, **91**, 4100–4106.
33 J. X. Liu, Q. L. Deng, D. Y. Tao, K. G. Yang, L. H. Zhang, Z. Liang and Y. K. Zhang, *Sci. Rep.*, 2014, **4**, 5487.
34 M. Dabrowski, M. Cieplak, P. S. Sharma, P. Borowicz, K. Noworyta, W. Lisowski, F. D'Souza, A. Kuhn and W. Kutner, *Biosens. Bioelectron.*, 2017, **94**, 155–161.
35 C. Armutcu, E. Özgür, M. E. Çorman and L. Uzun, *Colloids Surf., B*, 2021, **197**, 111435.
36 E. Yilmaz, K. Haupt and K. Mosbach, *Angew. Chem., Int. Ed.*, 2000, **39**, 2115–2118.
37 X. T. Shen and L. Ye, *Macromolecules*, 2011, **44**, 5631–5637.
38 S. T. Zhang, Q. Liu, S. Y. Jin, Yu. F. Bai, X. J. Feng and G. Q. Fu, *Talanta*, 2021, **234**, 122690.
39 J. Blümmel, N. Perschmann, D. Aydin, J. Drinjakovic, T. Surrey, M. Lopez-Garcia, H. Kessler and J. P. Spatz, *Biomaterials*, 2007, **28**, 4739–4747.
40 S. Nestora, F. Merlier, S. Beyazit, E. Prost, L. Duma, B. Baril, A. Greaves, K. Haupt and B. Tse Sum Bui, *Angew. Chem., Int. Ed.*, 2016, **55**, 6252–6256.
41 S. J. Zhu, Q. N. Meng, L. Wang, J. H. Zhang, Y. B. Song, H. Jin, K. Zhang, H. C. Sun, H. Y. Wang and B. Yang, *Angew. Chem., Int. Ed.*, 2013, **52**, 3953–3957.
42 M. J. Cho and S. Y. Park, *Sens. Actuators, B*, 2019, **28**, 719–729.
43 W. Stöber, A. Fink and E. Bohn, *J. Colloid Interface Sci.*, 1968, **269**, 62–69.
44 S. Berger, A. Synytska, L. Ionov, K. J. Eichhorn and M. Stamm, *Macromolecules*, 2008, **41**, 9669–9676.
45 C. Kaewsaneha, P. Tangboriboonrat, D. Polpanich, M. Eissaa and A. Elaissari, *Colloids Surf., A*, 2013, **439**, 35–42.
46 M. Lattuada and T. A. Hatton, *Nano Today*, 2011, **6**, 286–308.
47 A. Perro, F. Meunier, V. Schmitt and S. Ravaine, *Colloids Surf., A*, 2009, **332**, 57–62.
48 G. T. Hermanson, *Bioconjugate Techniques*, 2nd edn., Academic Press, London, 2008.
49 K. J. Hwang and P. Y. Sz, *Chem. Eng. J.*, 2011, **166**, 669–677.
50 Q. Yang, J. H. Li, X. Y. Wang, H. L. Peng, H. Xiong and L. X. Chen, *Biosens. Bioelectron.*, 2018, **112**, 54–71.
51 X. Han, W. Y. Han, S. T. Zhang, Z. Q. Liu and G. Q. Fu, *RSC Adv.*, 2019, **9**, 38165–38173.
52 Z. Zhang, J. H. Li, X. Y. Wang, D. Z. Shen and L. X. Chen, *ACS Appl. Mater. Interfaces*, 2015, **7**, 9118–9127.
53 D. Y. Li, X. W. He, Y. Chen, W. Y. Li and Y. K. Zhang, *ACS Appl. Mater. Interfaces*, 2013, **5**, 12609–12616.
54 X. Y. Wang, S. M. Yu, W. Liu, L. W. Fu, Y. Q. Wang, J. H. Li and L. X. Chen, *ACS Sens.*, 2018, **3**, 378–385.
55 J. A. Tan, M. L. Guo, L. Tan, Y. Y. Geng, S. Y. Huang, Y. W. Tang, C. C. Su, C. C. Lin and Y. Liang, *Sens. Actuators, B*, 2018, **274**, 627–635.
56 C. H. Sun, L. L. Pan, L. Zhang, J. J. Huang, D. D. Yao, C. Z. Wang, Y. Zhang, N. Jiang, L. N. Chen and C. S. Yuan, *Analyst*, 2019, **144**, 6760–6772.
57 W. Zhang, X. W. He, Y. Chen, W. Y. Li and Y. K. Zhang, *Biosens. Bioelectron.*, 2011, **26**, 2553–2558.
58 C. C. Yang, X. M. Yan, H. Guo and G. Q. Fu, *Biosens. Bioelectron.*, 2016, **75**, 129–135.
59 W. Li, Y. Sun, C. C. Yang, X. M. Yan, H. Guo and G. Q. Fu, *ACS Appl. Mater. Interfaces*, 2015, **7**, 27188–27196.
60 Y. Inoue, A. Kuwahara, K. Ohmori, H. Sunayama, T. Ooya and T. Takeuchi, *Biosens. Bioelectron.*, 2013, **48**, 113–119.